University of California, San Diego UCSD-CER-05-06

Comprehensive and reliable diagnostics for the corona of laser-produced plasmas

Y. Tao, M. S. Tillack, S. S. Harilal,
B. O'Shay, K. Sequoia, and F. Najmabadi

September, 2005

Center for Energy Research
University of California, San Diego
9500 Gilman Drive
La Jolla, CA 92093-0420

Comprehensive and reliable diagnostics for the corona of laser-produced plasmas

Y. Tao, M. Tillack, S.S. Harilal, B. O'Shay, K. Sequoia, and F. Najmabadi
Mechanical and Aerospace Engineering Department
and the Center for Energy Research
University of California, San Diego

Abstract: Comprehensive and reliable diagnostics for the corona of laser-produced plasmas, including optical interferometry, Shack Hartmann wave-front sensor (SHWS), Thomson scattering, 13.5 nm extreme ultraviolet (EUV) shadowgraphy, and x-ray absorption spectroscopy are proposed to be developed utilizing a small scale, affordable experimental platform, which consists of a 500 mJ/150 ps commercial Nd:YAG laser, a 650 mJ/7 ns Nd:YAG laser and a vacuum chamber with a diameter of 40 cm. SHWS and 13.5 nm EUV shadowgraphy are completely new technologies, and SHWS has a great potential to be extended into x-ray wavelengths with low cost. A comprehensive set of plasma parameters in the corona including electron and ion density profiles, temperature profile, and ionization charge state distribution etc. with high spatial and temporal resolutions will be measured. Results from various methods can be compared with each other (for example, electron density profile can be measured by both interferometry and Hartmann wave-front sensor, ion density by both 13.5 -nm EUV shadowgraph and x-ray absorption spectroscopy, temperature by both Thomson scattering and x-ray absorption spectroscopy), such that more reliable data can be expected. This research will provide comprehensive and reliable experimental plasma parameters in the corona to benchmark hydrodynamic and atomic codes, which play a key role in designing laser plasma interaction experiments in the fields of 13.5nm EUV lithography (EUVL) source, soft x-ray source, and research relevant to laser fusion etc. Technologies, facilities, and experiences of plasma diagnostics will be developed and accumulated, fostering opportunities to carry out research on plasma diagnostics in the field of laser fusion, high energy density physics, and magnetic confinement fusion.

1. Background

High power laser produced plasmas (LPPs) are highly transient media with high gradients both in temperature and density, having various applications in a wide range of fields, like nuclear fusion energy, biology, life science, material science, and the semiconductor industry [1][2][3] etc. Knowledge of the plasma parameters is fundamental to understanding physical processes in laser plasma interactions, which have a long history and have been greatly motivated by research on laser fusion and x-ray lasers [4][5]. However, because of the large variety of materials, various application fields under a wide range of experimental conditions, and the complexity arising from steep gradients in density and temperature profiles, plasmas diagnostics has been one of the most active areas in modern physics until now [6][7][8], especially for some high Z materials that are interesting in specific applications of extreme ultraviolet lithography (EUVL), soft x-ray sources, and laser plasma interactions related with laser fusion. Because most of the previous diagnostics were carried out using large-scale laser facilities, especially when comprehensive and reliable parameters with temporal and spatial resolutions were required, most of the efforts focused on a limited number of materials in limited fields, like laser fusion, x-ray lasers etc. In fact, a wide range of applications of LPPs are being investigated in a huge number of small groups distributed widely through universities and industry. Most of the small group can't afford expensive, complicated, and large scale laser facilities. And the small available laser energy limits the achievable plasma size in some applications, making detailed diagnosis a challenge. So there is a great need to demonstrate comprehensive and reliable diagnostics utilizing a compact, affordable laser system, so that the diagnostics can be applied to wide application fields under various experimental conditions.

The corona is the region from well under-dense to critical density in laser-produced plasmas. Most of the important phenomena of laser plasma interaction, like absorption of laser energy, ionization, radiation generation and transport, and nonlinear scattering etc., occur in this region. And most of the radiation in the EUV and soft x-ray wavelength range (1-100 nm) comes from this region. Therefore, well-characterized corona parameters are necessary for the applications of EUVL sources, intense soft x-ray sources, and laser fusion.

EUVL will hopefully be next generation lithography tool in the semiconductor industry for fabricating several 10 nm electronic nodes. However, challenges must be addressed before applying it to mass-production. One is development of a powerful, efficient, clean, and long lifetime 13.5 nm EUV light source. Laser produced Sn-based plasma has been one of the most promising sources, it has shown the highest conversion efficiency until now, 3% in 2% bandwidth [9]. But the physics of

generation and transport of 13.5 nm EUV light in laser produced Sn-based plasmas has never been completely understood, because of the huge number of transitions in a high Z material and steep gradients in density and temperature. There is a great need to validate hydrodynamic and atomic codes employed to optimize EUVL LPPs with reliable and comprehensive measurements of plasma parameters. Previous works have shown that efficient 13.5 nm EUV light mainly comes from the corona in Sn-based plasmas due to less opacity [6][10]. Low density Sn-doped foam target has shown comparable conversion efficiency with solid density Sn with much less debris from Sn, and additional C and O particles can be mitigated efficiently by ambient gas, magnetic, and electric fields etc. However most of the efforts in developing EUVL sources focus on characterization of properties of EUV light [11][12][13], there are very few experimental data of plasma parameters, especially for low density Sn-based targets.

Soft x-rays in a wide wavelength range generated from laser-produced plasmas have many applications in microscopy, lithography, and surface modification of materials. Wavelengths located between the k-edges of carbon (284.2 eV) and oxygen ions (543.1 eV) are called the water window, having a great potential to be applied to x-ray microscopy in life sciences because of their high contrast between water and organic tissues. Understanding and optimizing plasma physics are critical to develop an efficient, clean, and long-life time soft x-ray source for these applications [2][14]. For example, there has been a long history to optimize density profile to achieve high conversion efficiency, however there are few data to characterize the density profile and correlate it with the properties of x-rays.

Laser plasma interactions in the corona are also important to laser fusion, because the National Ignition Facility (NIF) target designs use hohlraums filled with gas [15], in which focused high intensity laser beams ionize the gas and pass through the corona to reach the radiation-converting wall. Plasma parameters in the corona, such as density and temperature profiles, play an important role in the generation of scattering light and the formation of filaments, which influence laser beam transport and result in asymmetry of irradiation. Recently, there has been an intention to use 2ω light to achieve ignition, because of higher available laser energy. However, most of the previous work on laser plasma interactions using the Nova facility focused on ultraviolet light, so investigation on the interaction of green laser light with coronal plasmas has become a hot topic in laser fusion research [8][16].

Hydrodynamic and atomic codes are standard tools to understand and to optimize the physics of laser plasma interactions. Hydrodynamic codes include LASNEX [17], ILESTA [18], MEDUSA [19],

HYADES [20], and HELIOS [21] etc. Atomic codes include COWAN [22], FLY [23], Cretin [24] and SPECT 3D [21] etc. However to date, it is still hard to compare experimental and simulation results for some specific materials under the specific experimental conditions, such as laser-produced Sn-based plasmas for EUVL source [25] and radiation transport in laser-produced metal doped foam plasma related with laser fusion [26], the reason is the availability and accuracy of experimental data under the corresponding experimental conditions.

The purpose of this proposal is to demonstrate comprehensive diagnostics for the corona of laser-produced plasmas utilizing a compact and affordable experimental platform. We will provide reliable-experimental data to benchmark hydrodynamic and atomic codes used to understand and to design laser plasma interactions related with EUVL sources, laser fusion, and soft x-ray sources. We will describe the lasers and vacuum chamber used in experiments. The principle, feasibility, advantages, and experimental arrangement of the diagnostics, including optical interferometry, Shack Hartmann wave front sensor, Thomson scattering, 13.5 nm EUV shadowgraphy, x-ray absorption spectroscopy, and others, will be discussed in this report.

2. Lasers and vacuum chamber

Because intense laser-produced plasma is highly transient, a short pulse probe beam is required to avoid time-integration effects. Temporal evolution of plasma arises from two facts: one is the specified temporal profile of the laser pulse and the other is rapid thermal expansion arising from high gradients both in density and temperature. As an example, for EUVL source plasmas, typical pulse widths of laser pulses are 5-10 ns (10^{-9} s); sub-ns is short enough to distinguish the phenomena occurred at different times within laser pulse. The thermal expansion velocity in the corona can be described as, $C_s = \sqrt{ZT_e / M}$ in which Z, T_e and M_i are the average charge state, plasma temperature, and mass of ions. Typical plasma temperatures favorable for efficient 13.5 nm EUV light are from 30 to 60 eV. The preferred averaged ionization state is $Z = 10$, and C_s is about several times 10^{6} cm/s. If spatial resolution around several micrometers is required, then a pulse duration of ~100 ps is required. D.S.Montgomery et al [27] have shown that a steady plasma state can be achieved within 200 ps for plasma generated by ns laser.

Using a short pulse, temporal resolution can be achieved by verifying the delay time between the pump and probe laser pulses. Critical density and refraction effects require short

wavelength. Interferometry and SHWS require very small laser energy, but Thomson scattering, x-ray shadowgraphy and x-ray absorption spectroscopy require relatively large energy.

The EKSPLA SL335/SH [28] will be employed as the probe laser. This picosecond (10^{-12} s) Nd:YAG laser consists of a self-seeded Q-switched master oscillator, a stimulated Brillion scattering (SBS) compressor, and two stages of power amplifiers. It produces 1.064 μm laser pulses at with pulse energy of 500 mJ, pulse duration varying from 150 to 550 ps. When it is used as probe laser, the shortest pulse duration is always selected. Second and fourth harmonics are available, the corresponding energies are 240 and 60 mJ respectively. The line width is less than 0.1 cm^{-1} at 1.064 μm. The near field pattern is close to Gaussian as illustrated in Fig. 1. If the beam divergence is less than 0.5 mrad, then intensity on the target up to 1×10^{14} W/cm^2 can be expected using a focus lens with focal length of 100 mm. Short pulse and low external triggered jitter (<0.5 ns) enable high time resolution to perform research utilizing double pulses by synchronizing with another ns laser.

Plasmas will be generated by the EKSPLA laser or by a ns Nd:YAG laser. The ns laser provides 1.064 μm pulses with energy of 650 mJ, pulse duration of 7 ns, at 10 Hz. In experiments, laser intensities on the target can be varied from 10^{10} to 10^{14} W/cm^2, pulse durations from 150 ps to 7 ns. Experiments under favorable conditions for EUVL sources, soft x-ray sources, and laser plasma interactions related to laser fusion will be carried out. The two lasers are synchronized with jitter less than 0.5 ns. The jitter is also monitored by a fast photodiode equipped with a 500 MHz digital oscilloscope.

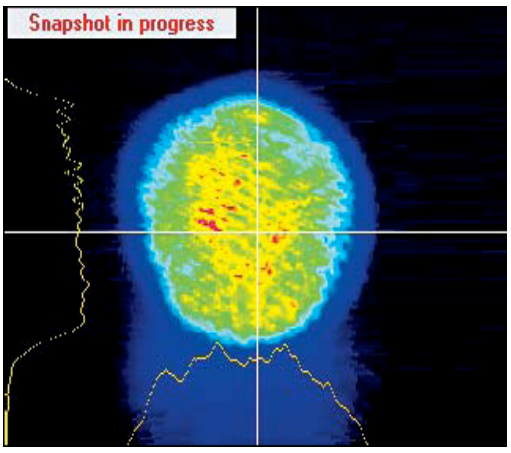

Fig.1 Near field pattern of SL335/SH laser beam

A vacuum chamber with 40 cm diameter and vacuum below 10^{-6} Torr will be employed to contain the laser plasma interactions. An automated target positioning system suitable for high repetition rate operation will enable accurate positioning in three dimensions. Two monitor cameras in two directions, i.e. normal view and side view, will be installed. The resolution of the target position and monitor system is less than 20 μm.

3. Diagnostic technologies to be developed

3.1 Optical Interferometry

Optical interferometry is a convenient means to deduce **electron density profile** in the under dense region [4]. The phase variation induced by plasma is recorded in an interferogram, and is related with the electron density n_e by,

$$\delta\varphi(x,y) = \frac{2\pi}{\lambda}\int_0^L [n(x,y,z)-1]dz \quad (1)$$

where $n = (1 - n_e / n_c)^{1/2}$ is the refractive index of plasma , and $n_c = 1.1\times10^{21}\lambda^{-2}$ is the critical density with the probe wavelength λ in micrometers. Short probe wavelength allows access to higher plasma density, and longer wavelength is preferred to obtain a significant phase shift in the under-dense region.

Relatively large-scale plasma size is required for efficient EUVL sources [9] and laser fusion research, and there is a steep gradient in density profile. The refraction induced by the electron density gradients can't be neglected and limits the application of interferometry in these cases. Rays associated with the probe beam that initially propagate parallel to the target surface will bend toward regions of low density. This introduces two effects on the interferogram: one is the limitation of the accessible maximum density because of finite collection angle of the imaging optics, and the other is the error on spatial resolution. The angle of refraction may be approximated as[29],

$$\theta = L\left(\frac{n_e(z)}{n_c l_s}\right) \quad (2)$$

where L is the length of plasma, z is the distance from the target, and l_s is the scale length of plasma. Assume that the plasma density profile is given as, $\mathbf{n_e(z) = n_{e0}\ exp(-z/l_s)}$. Then the error σ induced by the deflection of the rays can be approximated as $\boldsymbol{\sigma = L \bullet \theta}$. For L ~ 300 μm, in order to control the total error under 20 μm, the error of refraction should be less than < 15 μm, so that θ<0.05. The maximum accessible electron density n_e is ~ 6×10^{19}cm^{-3} for a 532nm probe beams by assuming $l_s \sim 200\ \mu m$. As such, F/20 imaging lenses are used.

An experimental arrangement using a polarization interferometer is illustrated in Fig.2. A small part split from the EKSPLA laser beam is converted into 2ω (532 nm) by a type II KDP crystal and used as probe beam. A λ/2 wave plate and polarizer are used to adjust the energy and rotate the polarization of the probe beam. The polarization is set at an angle of 45 degrees with respect to the optical axis of a Wollaston prism. A convex F/20 lens relays the plasma image to the imager (visible CCD camera). The Wollaston prism splits the probe beam into two beams with orthogonal polarization. The second polarizer is used to adjust the intensities of the two beams to achieve equal intensity and equal polarization in the overlap area. In this arrangement, the part distorted by the plasma contained in one beam will interfere with the un-distorted part of the other beam. A narrow band interference filter is employed to shield the detector from plasma emission.

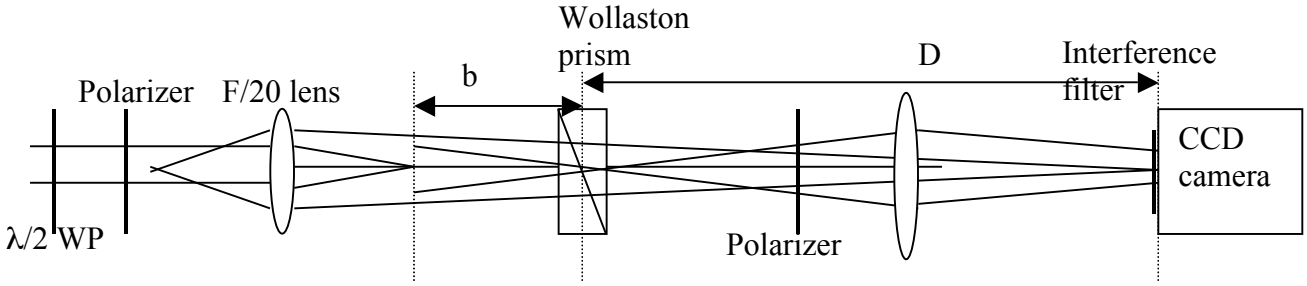

Fig.2 Experimental arrangement of polarization interferometer

The fringe distance is determined by, $\delta i = \dfrac{D}{b \bullet \varepsilon}\lambda$, where D is the distance from the prism to the imager, b is the distance from the rear focus of the imaging lens to the prism, and ε is the split angle of the Wollaston prism. In our arrangement, b can be varied from 200 to 400 mm, b+D=900 mm, ε=10 mrad, then $\delta i = 75 - 150 \mu m$ (in the image plane), and $\delta i = 7.5$~15μm (in the target plane). The magnification is given by, $M = \dfrac{f + b + D}{f} = 10$, where f=100 mm is the focal

length of the imaging lens. Recalling the error induced by refraction, the spatial resolution will be about 20 μm, and will be calibrated in experiments. The temporal resolution will be better than 200 ps by monitoring the jitter between probe and pump laser pulses. If the size of the CCD camera is 8×8mm, the field of view on the target is 800 μm. The probe beam size will be 2-3 mm.

The phase shift is extracted by mathematical treatment based on the Fast Fourier Transform (FFT) method from two interferograms [30]; one is obtained with plasma and the other is obtained without plasma (the reference). The intensity profile of the interfergram containing the distorted phase induced by plasma can be described as,

$$\mathbf{I(z_i,x) = 2I_0(z_i,x) + c(z_i,x)\exp[2\pi f_0 x)] + c^*(z_i,x)\exp[-2\pi f_0 x)]} \qquad (3)$$

with $\mathbf{c(z_i,x) = I_0(z_i,x)\exp[i\Delta\phi(z_i,x)]}$, and its conjugate c* contains all the information relative to the phase shift $\Delta\varphi$ induced by the plasma. f_0 is the spatial frequency of fringes. 1-D FFT with respect to the x-axis is applied,

$$\mathbf{F(z_i,f) = F_0(z_i,f) + C(z_i,f - f_0) + C^*(z_i,f + f_0)} \qquad (4)$$

Since the spatial frequencies of $\mathbf{I_0(z,x)}$ and $\mathbf{\phi(z,x)}$ are much lower than $\mathbf{f_0}$, the Fourier spectra are separated by $\mathbf{f_0}$. $\mathbf{C(z_i,f - f_0)}$ contains all the desired information ; the other two items in equation (4) are shielded away. Unwanted background signal is removed in this process. The inverse FFT of C in the plasma case gives, $\mathbf{c_p(z_i,x) = I_0(z_i,x)\exp[i\phi(z_i,x)]}$. And the i nverse FFT of this component in the reference interferogram gives, $\mathbf{c_r(z_i,x) = I_0(z_i,x)}$. Then the phase shift is obtained from the imaginary part of the logarithm of the ratio $\mathbf{Image[\log(c_p / c_r)]}$.

Laser-produced plasmas are often cylindrically symmetric, so that Abel inversion can be used to extract a density map from the phase map. The symmetric axis is the x axis (along the laser incidence line). By using Abel inversion, the equation can be rewritten as

$$\mathbf{k_0[n(r,x) - 1] = -\frac{1}{\pi}\int_r^{r_0}\left[\frac{d\phi(z,x)}{dz}\right]\frac{dz}{\sqrt{z^2 - r^2}}} \qquad (5)$$

$$\mathbf{n_e(r,x) = -\frac{\lambda}{\pi}n_c\int_r^{r_0}\left[\frac{d\phi(z,x)}{dz}\right]\frac{dz}{\sqrt{z^2 - r^2}}} \qquad (6)$$

Interferometer Data Evaluation Algorithm (IDEA) will be used to calculate the Abel inversion[30], where f-interrogation and FFT methods are adopted. The number of the cubic polynomial was optimized for each line.

Using this method, measurements of electron density profile of laser-produced plasma related with 13.5 nm EUVL source will be performed. Various targets, such as, bulk solid density Sn, foil Sn, thin coating Sn, low density Sn-doped foam, and Li targets will be investigated. The relation between the properties of 13.5 nm EUV light and plasma density profile will be examined in detail. Effects of plasma density profile on soft x-ray generation will be checked. The transport of high intensity laser in underdense plasma will be studied, which is related with indirect-drive ignition of laser fusion.

3.2 **Hartmann wave-front sensor**

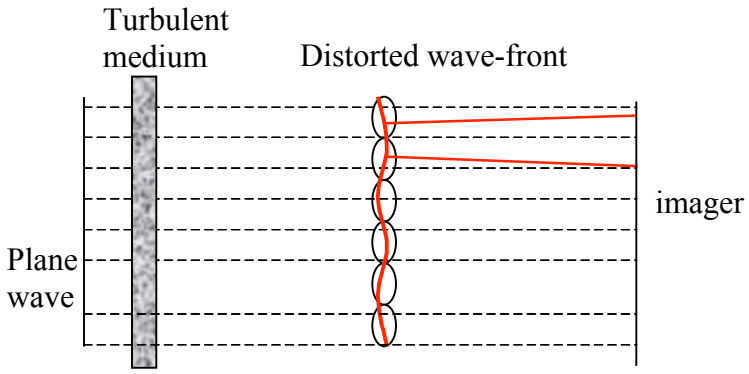

Fig. 3 Principle of Hartmann wavefront senor

A wave-front is the surface in which all of the points have the same phase. Light waves can be divided into plane, spherical, and others waves corresponding to their wave front. The central part of a Shack Hartmann wave-front sensor (SHWS) is a micro lens array. A plane wave incident on a SHWS is broken into beamlets and produces an array of spots located on the optical axis (dash line) of an individual lens on the imager, as illustrated in Fig. 3. When the light passes through a non-uniform medium, such as a turbulent atmosphere, phase distortion will be added to the wave front of the incident light beam. The distorted wave-front produces a local gradient in the phase, $\nabla\phi$, displacing the spot from the axis, shown as the red line. Each individual spot is displaced from the axis by a distance $s = \frac{\nabla\phi \bullet f \bullet \lambda}{2\pi}$, where λ is the wavelength of the incident light and f is the distance from the Hartmann lens array to the detector. The individual spot displacement directly provides the corresponding phase tilt in the place of the lenslet, so that the distorted wave-front can be reconstructed. Comparison between

the incident wavefront and the distorted wavefront can provide the density distribution of the nonuniform medium.

There is a very steep density gradient in the laser-produced plasma. As light rays propagate through the plasma, their phase is altered by the gradient of electron density and the wavefront is distorted. A SHWS measures the local wavefront tilt perpendicular to the probe light, if the probe light passes through the plasma perpendicular to the plasma expanding direction, A SHWS can provides the 2-D density gradient distribution in the plane x-y, where x is the expansion direction and y is parallel to the target surface [31]. The local phase tilt due to a plasma gradient is given by

$$\nabla k = \frac{2\pi}{\lambda}\nabla n = -\frac{\omega}{c}\frac{1}{2}\frac{1}{\sqrt{1-\frac{n_e}{n_{cr}}}}\frac{1}{n_{cr}}\nabla n_e \qquad (7)$$

The feasibility of SHWS to measure phase distortion induced by a programmable liquid crystal has been demonstrated [32].

In principle, a SHWS can easily be extended into x-ray wavelengths, because it does not require coherent light. Under the benefit of efforts of EUVL source development, a bright 13.5 nm EUV light based on a small-scale commercial laser is ready to be used. And multi-layer EUV mirrors with high reflectivity at normal incidence are commercially available, which can collect, collimate, and focus 13.5 nm EUV beam with high transport efficiency. Due to small refraction and high corresponding critical density (6×10^{-24} cm^{-3}), 13.5 nm EUV light can penetrate the dense plasma region. It will be a powerful and low cost tool to diagnostic plasma density profile in dense region compared with x-ray laser interferometer, which requires complicated experimental arrangement and a large-scale laser facility [33][34]. Dense region of LPPs is greatly interesting in the fields of laser fusion, high energy density physics etc.

For an EUV SHWS the only difference from the visible version is the ‘micro-lens array’. For EUV light, reflective mirrors can only be used because of its heavy absorption in any materials. Fortunately, multi-layer Mo/Si coating are commercially available on various substrates [35], which has a 70% reflectivity centered at 13.5 nm at normal incidence, so a micro concave spherical mirrors array coated with multiplayer Mo/Si coating is affordable and will be used as a ‘micro lens array’. Another choice for EUV ‘micro lens array’ is a Hartmann mask.

Until now, there is no experimental measurement on practical plasma using SHWS even with visible light. So first, it is important to demonstrate its ability to measure real density profiles of LPPs. The feasibility of this technique applied to practical laser-produced plasmas will be examined, experiences for system design will be accumulated, and software for data processing will be developed with a very low cost. If successful, it will be become much easier to find funding to extend this new technology to x-ray wavelengths. Designation of 13.5 nm EUV SHWS will be performed.

The experimental arrangement is similar to interferomery: a small part of the laser beam split from the EKSPLA laser will be converted into 2ω (532 nm) and used as a probe beam. The probe beam passes through plasma and is relayed to a SHWS. A SHWS facility (CLAS-2D from Wavefront Science Inc.) in the laser laboratory at UCSD will be employed. An automatic code will be developed and employed to extract a phase map from SHWS. Abel inversion will be employed to achieve density map. Measurement of electron density profile using SHWS for laser-produced plasmas under the favorable conditions for efficient 13.5 nm EUVL source will be carried out. The results will be compared to the results from optical interferometry under the same conditions.

3.3 Thomson scattering

Laser-based Thomson scattering (TS) provides a wavelength shift due to electron motion in the local electric field [36]. It has been adopted as a fundamental diagnostic of plasma parameters and basic processes in laser produced plasmas [37], because its data processing does not depend on complicated models compared with other methods, like x-ray spectroscopy [38]. Electron temperature, T_e, electron density, n_e, the averaged ionization stage, $\bar{Z}$, ions temperatures, T_i, and relative ion concentration of plasma can be measured with high accuracy [37].

TS is characterized by the scattering parameter α, which is proportional to the ratio of the probe scale length $\lambda_s = \frac{\lambda_{probe}}{2}\sin(\theta/2)$ to the Debye length, $\alpha = \frac{\lambda_s}{2\pi\lambda_D}$, where Debye length is given by $\lambda_D(cm) = \sqrt{\frac{T_e}{4\pi n_e e^2}} = 743(\frac{T_e[ev]}{n_e[cm^{-3}]})$. For $\alpha < 1$, it is collisional collective TS, for $\alpha > 1$, it is called collective TS. Our plasmas of interest, with low density and moderate or high temperatures, fall into the collective scattering regime. The dominant source of scattering comes

from correlated long-wavelength density fluctuations rather than random motion of individual electrons (ions), i.e., scattering is dominated by high-frequency electron plasma waves (EPW or Langmuir wave) and low-frequency ion acoustic waves (IAW).

The spectrum induced by IAW will be characterized by two shifted peaks, one is red shifted ($\omega_{ia} = -k_{ia}c_s$) and the other is blue shifted ($\omega_{ia} = k_{ia}c_s$), where k_{ia} is the scattering vector, and the frequency separation of the two peaks is twice the ion acoustic frequency ω_{ia},

$$(\frac{\omega_{ia}}{k_{ia}})^2 \cong \frac{T_e}{M_i}(\frac{\overline{Z}}{1+k_{ia}\lambda_D} + \Gamma_i \frac{T_i}{T_e}) \approx \frac{T_e}{M_i}(\frac{\overline{Z}}{1+k_{ia}\lambda_D}) \qquad (8)$$

where M_i is the ion mass, T_i is the ion temperature, Γ_i is the specific heat ratio, and the length of the scattering vector k_{ia} is given by the triangle relation shown in Fig. 4. For highly ionized plasma, $T_i << T_e$.

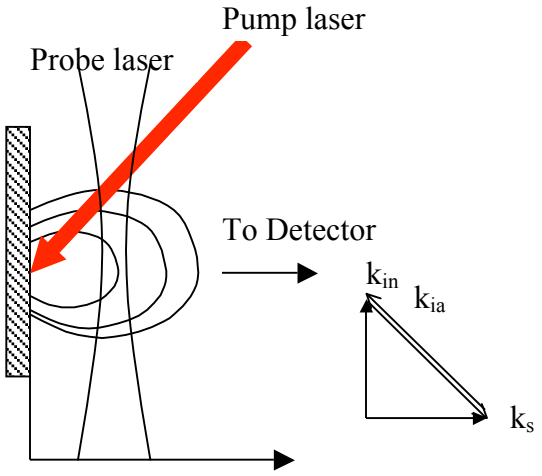

Fig.4 Illustration of experimental arrangement for Thomson Scattering.

The propagation direction of the ion acoustic wave in the plasma is determined by the scattering vector $\vec{k}_{ia} = \vec{k}_{scat} - \vec{k}_{in}$, where $\vec{k}_{scat}$ and $\vec{k}_{in}$ are wave vectors of scattered and incident light. The incident wave vector can be found from the dispersion relation for an EM wave in plasmas, $\omega_{incident} = \omega_p + k_{in}^2 c^2$, where ω_p is plasma frequency, c is the velocity of light, and

$$k_{in} = \frac{\omega_{in}}{c}\sqrt{1-\frac{\omega_p^2}{\omega_{in}^2}} = \frac{\omega_{in}}{c}\sqrt{1-\frac{n_e}{n_{cr}}}, \qquad (9)$$

where $n_e = \frac{m_e \omega_p^2}{4\pi e^2}$ is plasma density and $n_{cr} = \frac{m_e \omega_{in}^2}{4\pi e^2}$ is the critical density. Since the frequency of the scattered light is shifted only by the comparably small ion acoustic frequency, the wave number of the scattered light is given by $k_s \approx k_{in}$, then $k_{ia} = 2k_{in}\sin(\theta/2)$. The temperature and ionization state can be estimated from the frequency separation. However, accurate information can only be achieved by fitting the IAW spectrum using the following expression for the scattered power, P_s, into a solid angle $d\Omega$ per frequency range $d\omega$,

$$\frac{dP_s}{d\Omega d\omega} = \frac{\vec{k}_{in} \bullet \vec{k}_s}{2\pi} \frac{e^2}{m_e c^2} \int dx S(\vec{k}, \omega; x) n_e(x) \int dy dz \frac{c E_0^2(r)}{8\pi} \qquad (10)$$

where E_0 is the probe electric field and $(S(\vec{k}, \omega; x)$ is the dynamic form factor that accounts for ion-ion collisions having the following form,

$$S(\vec{k}, \omega) = \frac{4k_{ia}^2 [c_s^2 / (1 + k_{ia}^2 \lambda_D^2) + \nu_i] \gamma_{ia}}{(\omega^2 - k_{ia}^2 v_s^2)^2 + 4\omega^2 \gamma^2} \qquad (11)$$

where $v_s = [c_s^2 / (1 + k_{ia}^2 \lambda_D^2) + \Gamma_i v_{i_i}^2]^{1/2}$, $c_s = \sqrt{\bar{Z} T_e / M}$, $v_i = \sqrt{T_i / M}$. The damping of IAW, $\gamma_{ia} = 2k_{ia}^2 v_i^2 \, \mathrm{Re}\eta_i / 3\nu_i + (\pi/8)^{1/2} c_s k_{ia} \nu_s / \nu_e$ and the specific heat ratio, $\Gamma_i = 5/3 + 4\omega \, \mathrm{Im}\eta_i / 3\nu_i$ are defined by the frequency-dependent ion viscosity, $\eta_i = i\nu_i(\omega + i1.46\nu_i)/[(\omega + 1.2i\nu_i)(\omega + 1.46i\nu_i) + 0.23\nu_i^2]$, where the ion-ion collisional frequency $\nu_i = 4\sqrt{\pi}\, \bar{Z}^4 e^4 n_i \Lambda_i / 3M^{1/2} T_i^{3/2}$. A code to calculate the above formulas will be developed to fit the IAW spectrum.

Frequency shift induced by heavily damped electron plasma waves is achieved by the Bohm-Gross dispersion relation, $\omega^2 = \omega_p^2 + \frac{3k_{in}^2 T_e}{m_e}$. The simultaneous observation of IAW and EPW spectra offers a unique way to obtain T_e, n_e, and $\bar{Z}$ from TS alone. However, large laser pulse energy is required to observe EPW spectrum [37]. We intend to focus on IAW spectrum in this research.

Feasibility using a small energy probe beam

For 532nm probe light, under the conditions of elctron density $n_e=2\times10^{19}/cm^3$, temperature $T_e=60eV$, and ionization state $Z=10$, the approximate wavelength shift is $\Delta\lambda \sim 0.08nm$. Requirements on the linewidth of the probe beam and resolution of the spectrometer are less than 0.01nm. EKSAPLA laser's linewidth is less than 0.0025nm (0.1/cm at 532nm). For this research effort, we plan to use the ELIAS-II high resolution spectrometer obtained from Cymer Corp. The ELIAS-II provides a maximum spectral resolving power of 25 fm (http:/www.ltb-berlin.de/elias.html).

Because plasma emission generated by 1.064 μm pumping laser at intensities from 10^{11} to10^{13} W/cm^2 is almost a continuum, harmonics can be neglected. And there is only a very small wavelength deviation of scattered light from the probe light, so that a narrow bandpass filter ($\Delta\lambda$=1nm) at 532 nm can be employed to shield plasma emission. And we mainly focus on plasma generated by laser pulse with small energy, so that plasma emission is much lower than experimentsin laser fusion [39][40]. So scattered signal with high contrast ratio is possible using a relative low probe energy (< 100 mJ)[41].

In experiments, the laser beam from the EKSPLA laser is converted into green light (532 nm), and passes through the plasma along a line parallel to the target surface. Spatial resolution will be achieved by moving the focus of the probe beam along the line of plasma expansion. A mask with a 20 μm pinhole will be employed to define the scattering region. The scattered light is collected by a F/3 lens and relayed onto the slit of the spectrometer. Recalling the resolution of the target positioner and monitor, spatial resolution will be better than 30 μm. Temporal resolution depends on the pulse duaration of the probe beam (150 ps) and jitter (0.5 ns) between pump and probe pulses, so temporal resolution is 0.5 ns. The temporal resolution can be improved to less than 200 ps by monitoring the jitter using a fast photodiode.

3.4 13.5 nm EUV shadowgraphy

X-ray shadowgraphy is a general way to obtain **ion density** profiles of plasma. A probe x-ray beam (backlighter) with intensity I_0 passes through plasma along z parallel to the target initial surface, 2-D shadowgraph in the plane of x and y, where x is parallel to the target initial surface and perpendicular to z, y is the direction of plasma expansion. Its intensity is attenuated by absorption induced by ions in the plasma. The output intensity is described as,

$$\frac{I(x,y)}{I_0} = \exp[\alpha\rho(x,y,z)l(z)] \qquad (12)$$

where α , ρ , and l are absorption coefficient, density, and length of the plasma. In the experiment, input and output intensities are measured. If absorption coefficient and length are known, the ion density of the plasma can be achieved.

For a given wavelength of backlighter and assuming the absorption cross section does not depend on the temperature, only mass absorption is necessary to consider. Absorption coefficients at room temperature are well known and tabulated [42], so the product of length and density can be deduced. A spatially resolved device-a pinhole camera or concave MLM mirror is employed to relay the x-ray shadow image of the plasma to an imager, like an x-ray CCD camera. In this way, 2-D shadowgraphs are achieved. Assuming that laser-produced plasma obeys cylindrical symmetry, Abel inversion can be used to calculate the re-convolution to obtain ion 2-D spatially resolved density profile. Using a short pulse x-ray backlighter, temporal resolution can be achieved by verifying delay times between the backlighter driven laser pulse and the pump laser pulse.

The EKSPLA laser will be used to generate backlighter x-ray sources. Another ns laser will be employed to generate plasma, with the two lasers synchronized with jitter less than 0.5 ns. The jitter is monitored for each shot by a fast photodiode. Because of the limitation of driving laser energy, an efficient soft x-ray backlighter source is required. Fortunately, very efficient 13.5 nm EUV light has been demonstrated using a small laser energy and low intensity [9]. And again combining commercially available normal incident reflective mirrors enables a bright monochromatic EUV backlighter at much lower cost than convention x-ray backlighter [43]. The experimental arrangement of an EUV backlighter using a MLM focusing mirror is illustrated in Fig.5. And it is suitable for low-density plasmas with moderate temperatures; such plasmas have applications in EUVL source, soft x- ray source, and laser fusion. The specifications of x-ray shadowgraphy are, Spatial resolution <20 μm, temporal resolution < 0.2 ns.

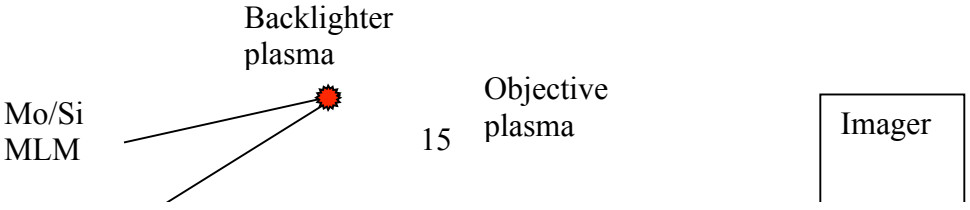

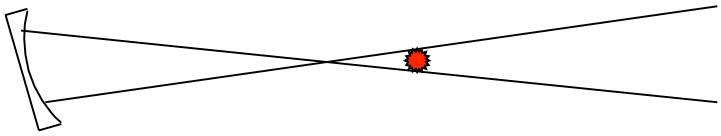

Fig.5 Principle illustration of bright EUV backlighter using MLM focus mirror

3.4 Spatially and temporally resolved x-ray absorption spectroscopy

X-ray absorption spectroscopy is a powerful tool for analyzing temperature, ionization state of ions, and density profiles of plasma. The absorption cross section of plasma can be measured in combination with atomic calculation [44,45]. It is also suitable to analyze the characteristics of the plume, which contains low charge state ions, and is important in debris characterization in EUVL sources plasmas and laser ablation.

The experimental arrangement is illustrated in Fig. 6. Semi-continuous x-ray light is generated by focusing the EKSPLA laser to a backlight target. After transmitting through the plasma to be investigated, the spectrum of x-ray light is recorded by a spatially resolved grazing-incidence spectrometer (GIS) equipped with a back-illuminated x-ray CCD camera. In this way, the spatially resolved absorption spectrum of the targeted plasma can be achieved. Temporal resolution is achieved by adopting the short pulse duration of the backligter x-ray driven by ps EKSPLA laser.

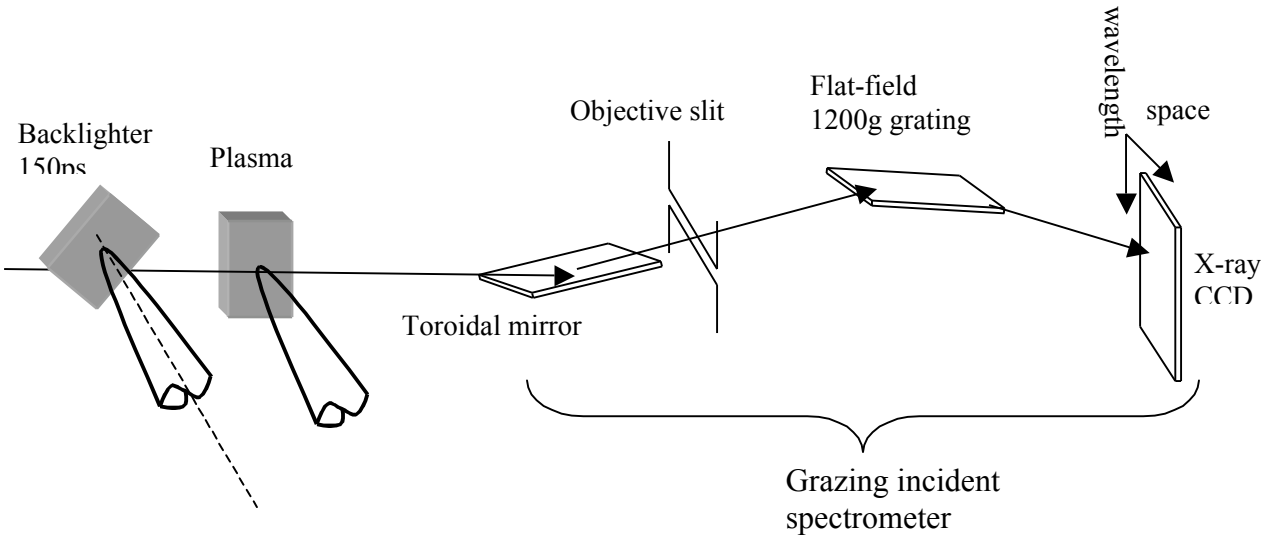

Fig.6 Experimental arrangement for spatial and temporal resolved x-ray absorption spectroscopy

For GIS, when using a spherical mirror as collecting optics, spatial resolution will be lost due to grazing incidence. Using toroidal focus mirror, stigmatic grazing incidence spectrometer can achieve spatial resolution around several 10μm [46].

3.5 Other diagnostics

3.5.1 Monochromatic EUV imaging

A concave spherical Mo/Si multilayer mirror will be employed to relay the plasma image to x-ray CCD camera or EUV light fluorescence glass (Cr:YAG) equipped with visible CCD camera. Monochromatic (13.5 nm ± 4%) EUV imaging can be taken with spatial resolution <10 μm and high light flux. This concave multi-layer mirror also can be used to focus EUV light; several μm spot size is easy to achieve. A high intensity, monochromatic 13.5nm EUV source is useful to carry out research on the modification and damage of surfaces induced by 13.5 nm EUV radiation, which have applications in material and life sciences. For example, a TW/cm^2 13.5 nm EUV light sources at 10 Hz can be realized using a commercial laser with 1J/10ns/10Hz.

Monochromatic EUV imaging can be used to characterize the process of radiation transport in LPPs, which is a basic process in laser plasma interaction [48][49][50]. Spatial profile of EUV emission along plasma density gradient will be investigated for low density Sn-based targets in order to clarify the effect of dominant emission region in density profile in low-density foam targets.

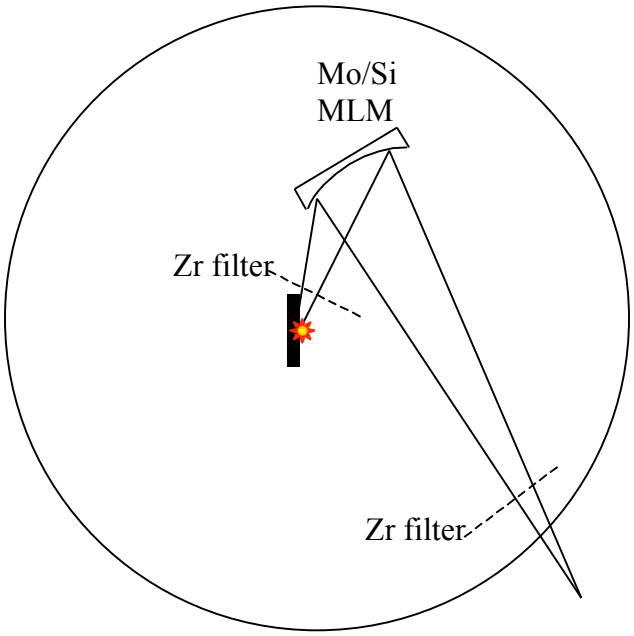

Fig.7. Illustration of monochromatic EUV imaging using concave MLM mirror

3.5.2 Movable Faraday cup

A movable Faraday cup will be built to study the properties of ions from laser-produced plasmas. Energy spectrum, angular distribution, and dynamics of ions in ambient gas will be investigated. Retarding voltage will be applied to analyze the charge state distribution.

3.5.3 Movable EUV energy monitor

A simplified EUV energy monitor will be developed, which consists of a concave spherical multi-layer Mo/Si EUV (NTT Corp.) mirror and a EUV filtered photodiode (International Radiation Inc.). The monitor will be calibrated by E-Mon from Jena Corp. It can be moved around the plasma, to measure the angular distribution of EUV light. The angular distribution is one of the important characteristics of EUV light and also must be included when conversion efficiency is calculated from E-Mon measurement, which is always fixed at a specific angle.

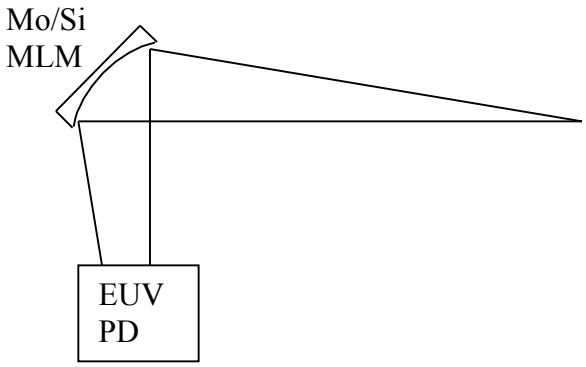

Fig.8 Illustration of movable EUV energy monitor

4. Expected results

Demonstration of novel diagnostics

This will be the first time to apply Shack Hartmann wave front sensor to plasma diagnostics. An assessment to extend it into EUV wavelength will be examined with low cost. Designation and development of data processing software for 13.5 nm EUV SHWS will be performed. Bright, compact, and low cost 13.5 nm EUV shadowgraphy will be demonstrated.

Facilities, technologies, and experiences on plasma diagnostics

Facilities, technologies, and experiences for plasma diagnostic will be developed and accumulated, which provide strong fundamentals to apply for funding to do further research on laser plasma interactions and their interactions in ‘big’ fields of plasmas, like laser fusion, high energy

density physics, magnetic confinement fusion, and x-ray source microscopy for material and biology sciences etc.

Reliable and comprehensive parameters

Comprehensive and reliable parameters of laser-produced plasma related with applications of EUVL source, soft x-ray sources, and laser fusion, including electron and ion density profile, temperature profile, and ionization charge state will be measured in a wide range of experimental conditions, which are greatly needed to benchmark hydrodynamic and atomic physics codes.

Reference:

1. Shalom Eliezer, The Interaction of High-Power Lasers with Plasmas. The Institute of Physics, London, 2002.
2. C. E. Turcu and J. B. Dance, X-Rays From Laser Plasmas : Generation and Applications. John Wiley & Sons, New York, 1998.
3. David Attwood, Soft x-rays and extreme ultraviolet radiation: Principles and Applications. Cambridge, New York, 2000.
4. I. H. Hutchinson, Principles of Plasma Diagnostics. Cambridge University Press, Cambridge, UK, 2002
5. A.Rubenchik and S. Witkowski, Physics of Laser Plasma, Elsevier Science Publishers B.V North-Holland 1991.
6. Y. Tao et al. Monochromatic imaging and angular distribution measurements of extreme ultraviolet light from laser-produced Sn and SnO_2 plasmas. Appl. Phys. Lett. 85, 1919 (2004)
7. Joshua B. Spencer, Darren A. Alman, David N. Ruzic, and Brian E. Jurczyk . Dynamics of a laser produced plasma for soft x-ray production .Proc. SPIE Int. Soc. Opt. Eng. 5751, 798 (2005).
8. C. Niemann et al. Intensity Limits for Propagation of 0.527 mu m Laser Beams through Large-Scale-Length Plasmas for Inertial Confinement Fusion. Phys. Rev. Lett. 94, 085005 (2005)
9. Y. Shimada, et al., Appl. Phys. Lett., 86 , 051501, (2005).
10. Y. Tao, H. Nishimura, S. Fujioka, A. Sunahara, M. Nakai, T. Okuno, N. Ueda, K. Nishihara, N. Miyanaga, and Y. Izawa. Characterization of density profile of laser-produced Sn plasma for 13.5 nm extreme ultraviolet source. Appl. Phys. Lett. 86, 201501 (2005)
11. R. C. Spitzer, T. J. Orzechowski, D. W. Phillion, R. L. Kauffman, and C. Cerjana, J.Appl.Phys. 79, 2251 (1996)

12. M. Richardson, C. Koay, K. Takenoshita, C. Keyser, and M. Al-Rabban, J.Vac.Sci.Technol. B22, 785(2004).
13. B. A. M. Hansson et al. Characterization of a liquid-xenon-jet laser-plasma extreme-ultraviolet source. Rev. Sci. Instrum. 75, 2122 (2004).
14. Joshua B. Spencer, Darren A. Alman, David N. Ruzic, and Brian E. Jurczyk. Dynamics of a laser produced plasma for soft x-ray production. Proc. SPIE Int. Soc. Opt. Eng. 5751, 798 (2005)
15. J. Lindl, Phys. Plasmas 2, 3933 (1995).
16. M. Stevenson et al., Phys. Plasmas 11, 2709 (2004).
17. J. A. Harte, W. E. Alley, D. S. Bailey, J. L. Eddleman, and G. B. Zimmerman. LASNEX—A 2-D PHYSICS CODE FOR MODELING ICF. UCRL-LR-105821-96-4 (1996).
18. Takabe H et al. Phys. Fluids 31, 2884(1988).
19. Christiansen, J.P. ; Ashby, D.E.T.F. ; Roberts, K.V. MEDUSA. A one-dimensional laser fusion code. Comput. Phys. Commun., 7,271(1974).
20. Cascade Applied Sciences, Inc.
21. Prism Computational Sciences, Inc., Madison, WI.
22. ftp://aphysics.lanl.gov/pub/cowan/
23. R. W. Lee et al., JQSRT 56:535-56. (1996).
24. H. A. Scott, "Cretin – a radiative transfer capability for laboratory plasmas," Journal of Quantitative Spectroscopy & Radiative Transfer **71** (2001) 689–701.
25. K. Nishihara et al. Modeling of LPP EUV Light Source at Japan MEXT Leading Project. 2004 EUVL International Symposium, Miyazakai, Japan.Nov.1-4,2004. So14. https://www.sematech.org/ euvlproceedings/
26. M.S Tillack, J. O'Shay, E. S. Simpson, C. A. Back and H. A. Scott. Radiation-hydrodynamic analysis of Ti-doped SiO2 aerogel exposed to 4-ns laser irradiation. UCSD technician report, UCSD-ENG-115, UCSD, 2005.
27. D.S.Montgomery, J.L.Kline, and T.E. Tierney IV. Detailed characterization of plasma wave behavior using collective Thomson scattering. Rev.Sci.Instrum. 75,3793 (2004).
28. EKSPLA, http://www.ekspla.com/
29. R.S.Smith, J.Dunn, J.Nilsen, J.R.Hunter, V.N.Shlyaptsev, J.J.Rocaa, J.Filevich, and M.C.Marconi. J.Opt.Soc.Am.B., 20,254(2003).
30. V.Malka, C.Coulaud, J.P.Geindre, V.Lopez, Z.Najmudin, D.Neely, F.Amiranoff. Rev.Sci.Instrum. 2329(2000).

31. http:/optics.tu-graz.ac.at/
32. K. L. Baker, J. Brase, M. Kartz, S. S. Olivier, B. Sawvel, and J. Tucker, Rev. Sci. Instrum. 73, 3784 2002.
33. K.L.Baker, J.Brase, M.Kartz, et al. Electron density characterization by use of a broadband x-ray-compatible wave-front sensor. Opt.Lett. vol.28, no.3, p149-151, 2003.
34. L. B. Da Silva et al. Electron Density Measurements of High Density Plasmas Using Soft X-Ray Laser Interferometry. Phys. Rev. Lett. 74, 3991 (1995)
35. J. J. Rocca, E. C. Hammarsten, E. Jankowska, J. Filevich, M. C. Marconi, S. Moon, and V. N. Shlyaptsev. Application of extremely compact capillary discharge soft x-ray lasers to dense plasma diagnostics. Phys. Plasmas 10, 2031 (2003)
36. http://www.ntt-at.com/products_e/multilayer/
37. J. Sheffield, Plasma Scattering of Electromagnetic Radiation. Academic, New York,1975.
38. S.H.Glenzer, et al. Thomson Scattering from laser plasmas. Phys.Plasma. 6, 2117 (1999).
39. Hans R.Griem. Principles of Plasma Spectroscopy. Cambridge University Press. London, UK. 1997.
40. S. H. Glenzer, L. M. Divol, R. L. Berger, C. Geddes, R. K. Kirkwood, J. D. Moody, E. A. Williams, and P. E. Young. Thomson Scattering Measurements of Saturated Ion Waves in Laser Fusion Plasmas. Phys. Rev. Lett. 86, 2565–2568 (2001).
41. A. J. Mackinnon et al. Implementation of a high energy 4 omega probe beam on the Omega laser. Rev. Sci. Instrum. 75, 3906 (2004)
42. M. D. Tracy, J. S. De Groot, K. G. Estabrook, andS. M. Cameron. Detailed 266 nm Thomson scattering measurements of a laser-heated plasma. Phys. Fluid B, 4, 1575,1992
43. http://physics.nist.gov/PhysRefData/XrayMassCoef/cover.html
44. D. K. Bradley, O. L. Landen, A. B. Bullock, S. G. Glendinning, and R. E. Turner. Efficient, 1--100-keV x-ray radiography with high spatial and temporal resolution. Opt. Lett. 27, 134 (2002)
45. Kouichi Murakami, Hans C. Gerritsen, Hedser van Brug, Fred Bijkerk, Frans W. Saris, and Marnix J. van der Wiel. Pulsed-laser irradiated silicon studied by time-resolved x-ray absorption (90–300 eV). Phys. Rev. Lett. 56, 655–658 (1986).
46. Katsuya Oguri, Yasuaki Okano, Tadashi Nishikawa, and Hidetoshi Nakano. Transient observation of extended x-ray absorption fine structure in laser-melted Si by using femtosecond laser-produced-plasma soft x ray. Appl. Phys. Lett. 87, 011503 (2005).

47. P. Villoresi and P. Nicolosi. Stigmatic spectrograph with a 2-D CCD detector for soft x-ray observations of laser produced plasmas. Rev.Sci.Instrum., 65, 2049(1994).
48. Y. Tao, M. Nakai, H. Nishimura, S. Fujioka, T. Okuno, T. Fujiwara, N. Ueda, N. Miyanaga, and Y. Izawa. Temporally resolved Schwarzschild microscope for the characterization of extreme ultraviolet emission in laser-produced plasmas. Rev. Sci. Instrum. 75, 5173 (2004).
49. Y.Tao et al. Dynamic imaging of 13.5-nm extreme ultraviolet emission from laser-produced Sn plasmas. Submitted to PRE.
50. M. Kado, K. A. Tanaka, R. Kodama, T. Yamanaka, and S. Nakai, K. Yamashita, M. Ohtani, and S. Kitamoto. Development of a Schwarzschild-type x-ray microscope. Opt.Lett., 16,109 (1991).